

# Pulmonary pathology of early-phase COVID-19 pneumonia in a patient with a benign lung lesion

Zhi Zeng,<sup>1</sup> Li Xu,<sup>1</sup> Xiao-Yu Xie,<sup>2</sup> Hong-Lin Yan,<sup>1</sup> Bao-Jun Xie,<sup>3</sup> Wan-Zhou Xu,<sup>4</sup> Xin-An Liu,<sup>5</sup> Gan-Jun Kang,<sup>6</sup> Wan-Li Jiang<sup>6</sup> & Jing-Ping Yuan<sup>1</sup>

<sup>1</sup>Department of Pathology, Renmin Hospital of Wuhan University, Wuhan, Hubei, <sup>2</sup>Department of Colorectal and Anal Surgery, Zhongnan Hospital of Wuhan University, Wuhan, Hubei, <sup>3</sup>Department of Radiology, Renmin Hospital of Wuhan University, Wuhan, Hubei, <sup>4</sup>Department of Clinical Laboratory, Renmin Hospital of Wuhan University, Wuhan, Hubei, <sup>5</sup>Brain Cognition and Brain Disease Institute (BCBDI), Shenzhen Institutes of Advanced Technology, Chinese Academy of Sciences, Shenzhen-Hong Kong Institute of Brain Science-Shenzhen Fundamental Research Institute, Shenzhen, and <sup>6</sup>Department of Thoracic Surgery, Renmin Hospital of Wuhan University, Wuhan, Hubei, China

Date of submission 1 April 2020

Accepted for publication 30 April 2020

Published online Article Accepted 6 May 2020

Zeng Z, Xu L, Xie X-Y, Yan H-L, Xie B-J, Xu W-Z, Liu X-A, Kang G-J, Jiang W-L & Yuan J-P.

(2020) *Histopathology* 77, 823–831. <https://doi.org/10.1111/his.14138>

## Pulmonary pathology of early-phase COVID-19 pneumonia in a patient with a benign lung lesion

**Aims:** An ongoing outbreak of 2019 novel coronavirus (CoV) disease (COVID-19), caused by severe acute respiratory syndrome (SARS) CoV-2, has been spreading in multiple countries. One of the reasons for the rapid spread is that the virus can be transmitted from infected individuals without symptoms. Revealing the pathological features of early-phase COVID-19 pneumonia is important for understanding of its pathogenesis. The aim of this study was to explore the pulmonary pathology of early-phase COVID-19 pneumonia in a patient with a benign lung lesion.

**Methods and results:** We analysed the pathological changes in lung tissue from a 55-year-old female patient with early-phase SARS-CoV-2 infection. In this case, right lower lobectomy was performed for a benign pulmonary nodule. Detailed clinical, laboratory and radiological data were also examined. This patient was confirmed to have preoperative SARS-CoV-2 infection by the use of real-time reverse tran-

scription polymerase chain reaction and RNA *in-situ* hybridisation on surgically removed lung tissues. Histologically, COVID-19 pneumonia was characterised by exudative inflammation. The closer to the visceral pleura, the more severe the exudation of monocytes and lymphocytes. Perivascular inflammatory infiltration, intra-alveolar multinucleated giant cells, pneumocyte hyperplasia and intracytoplasmic viral-like inclusion bodies were seen. However, fibrinous exudate and hyaline membrane formation, which were typical pulmonary features of SARS pneumonia, were not evident in this case. Immunohistochemical staining results showed an abnormal accumulation of CD4+ helper T lymphocytes and CD163+ M2 macrophages in the lung tissue.

**Conclusion:** The results highlighted the pulmonary pathological changes of early-phase SARS-CoV-2 infection, and suggested a role of immune dysfunction in the pathogenesis of COVID-19 pneumonia.

**Keywords:** 2019 novel coronavirus (SARS-CoV-2), COVID-19 pneumonia, macrophage, pathology, T lymphocyte

Address for correspondence: Jing-Ping Yuan, Department of Pathology, Renmin Hospital of Wuhan University, 99 Ziyang Road, Wuchang District, Wuhan 430060, Hubei Province, China. e-mail: yuanjingping2003@aliyun.com

Wan-Li Jiang, Department of Thoracic Surgery, Renmin Hospital of Wuhan University, No. 99, Ziyang Road, Wuchang District, Wuhan 430060, Hubei Province, China. e-mail: jiang\_wanli@163.com

## Introduction

Coronaviruses (CoVs) are enveloped, positive-sense, single-stranded RNA viruses that can infect human beings and many other vertebrates to cause respiratory, gastrointestinal and nervous system diseases.<sup>1–3</sup> In December 2019, an outbreak of the 2019 novel CoV disease (COVID-19), caused by severe acute respiratory syndrome (SARS)-CoV-2, attracted great attention from all over the world. As of 24:00 h on 23 April 2020, 82 804 confirmed cases and 4632 deaths had been reported in China.<sup>4</sup> The epidemic also spread rapidly in many other countries, such as the USA,<sup>5</sup> South Korea,<sup>6</sup> Italy,<sup>7</sup> and Iran,<sup>7</sup> posing a serious threat to human life and health. At present, urgent research on the aetiology, epidemiology, radiology, pathogenesis and therapeutics of this new CoV pneumonia is being carried out.<sup>8–10</sup> However, the pathological changes in the lungs caused by SARS-CoV-2, especially in the early stage of infection, have seldom been described.<sup>11,12</sup>

In this article, we have analysed the pathological changes in lung tissue from a COVID-19 patient. In this case, right lower lobectomy was performed for a benign pulmonary nodule. The patient was confirmed to have preoperative SARS-CoV-2 infection.

## Materials and methods

### PATIENT

The patient was a 55-year-old woman who lived in Wuhan. In May 2019 chest computed tomography (CT) showed a 7.5-mm ground-glass pulmonary nodule in her right lower lobe. On 14 January 2020, she came to hospital for further treatment, and the chest CT image showed that the pulmonary nodule had further increased in size to 10 mm (Figure 1A). The nodule was close to the hilum of the right lung. Except for the pulmonary nodule, she did not have any other comorbid conditions, such as hypertension,

diabetes, cardiovascular disease, and chronic obstructive pulmonary disease, and she did not have symptoms such as fever, dyspnoea, or cough on admission. Moreover, she had never smoked. She underwent right lower lobectomy on 17 January 2020. On the first postoperative day, her blood lymphocyte count decreased to  $0.82 \times 10^9/l$  (normal range:  $1.1–3.2 \times 10^9/l$ ). On the second postoperative day, she presented with a fever of  $38.5^\circ\text{C}$  without dyspnoea. On the third postoperative day, laboratory studies showed a white blood cell (WBC) count of  $3.09 \times 10^9/l$  (normal range:  $3.5–9.5 \times 10^9/l$ ) with  $0.76 \times 10^9/l$  lymphocytes. On the fourth postoperative day, she experienced slight dyspnoea without oxygen inhalation, and her blood oxygen saturation decreased to 95% (2 l/min, 29%). Real-time reverse transcription polymerase chain reaction (RT-PCR) showed positivity for SARS-CoV-2 RNA in a nasopharyngeal swab and sputum. Tests for influenza virus and other infectious agents gave negative results. Repeat chest CT showed patchy ground-glass opacity and focal consolidation with increasing density in the left and right lungs (Figure 1B). On the fifth postoperative day, the counts of peripheral blood CD3+, CD4+ and CD8+ T lymphocytes, and the serum IgG level, dropped dramatically. On the sixth postoperative day, her blood oxygen saturation decreased to 90% (4 l/min, 37%) and she developed a severe dry cough. One day later, the blood oxygen saturation fell below 55% (6 l/min, 45%), and she showed severe dyspnoea. She died before mechanical ventilation could be initiated. Following her death, two of her family members, one surgeon and four bedside nurses were confirmed to have SARS-CoV-2 infection (Figure 2).

### DATA COLLECTION

We reviewed and collected electronic medical records, pathological sections, laboratory findings and chest CT images of the patient. Two authors independently

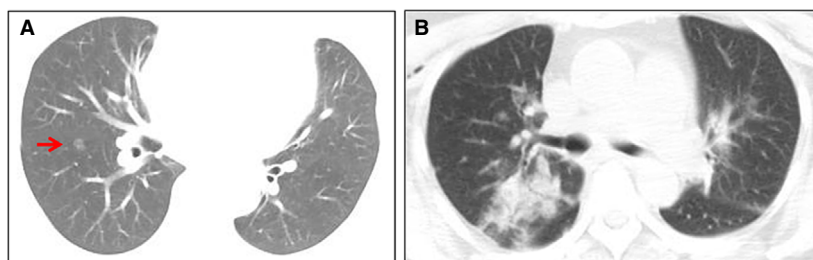


**Figure 1.** Chest computed tomography (CT) images before and after surgery. A, On 14 January 2020, the chest CT image showed a 10-mm pulmonary ground-glass nodule (arrow) in the right lower lobe. B, On 21 January 2020, the chest CT image showed patchy ground-glass opacity and focal consolidation with increasing density in the left and right lungs. [Colour figure can be viewed at [wileyonlinelibrary.com](http://wileyonlinelibrary.com)]

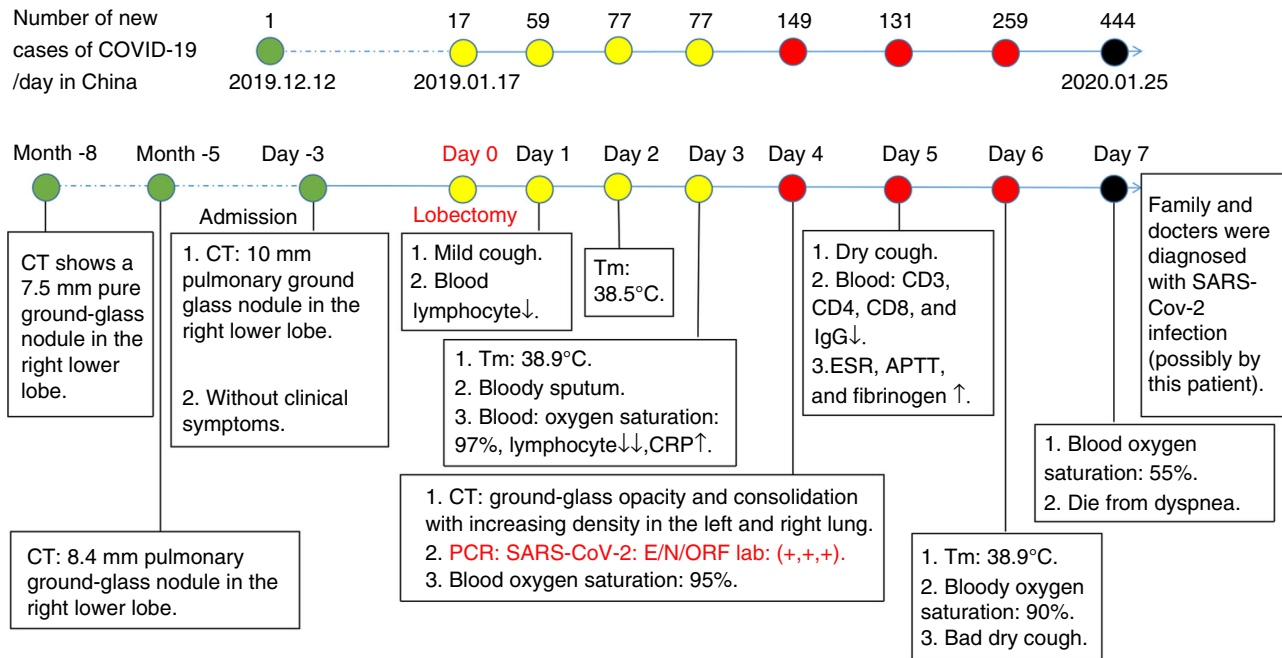


**Figure 2.** Clinical history and main laboratory findings. The patient underwent right lower lobectomy on 17 January 2020, and was diagnosed with 2019 novel coronavirus disease (COVID-19) on postoperative day 4 and died on postoperative day 7. [Colour figure can be viewed at [wileyonlinelibrary.com](http://wileyonlinelibrary.com)]

re-reviewed the collected data and pathological findings to confirm their accuracy.

#### HISTOPATHOLOGICAL EXAMINATION

Lung tissue was fixed with 4% neutral formaldehyde and embedded in paraffin wax, and 4- $\mu$ m sections were cut. Sections were stained with haematoxylin and eosin (H&E).

#### REAL-TIME RT-PCR

Real-time RT-PCR detection of SARS-CoV-2 in paraffin-embedded lung tissue was performed as described previously, with minor modifications.<sup>13</sup> In brief, deparaffinised and rehydrated tissue sections were homogenised in lysis buffer, and RNA was isolated with the AmoyDx FFPE RNA Kit (Cat No. 8.0224101X036G; Amoy Diagnostics, Xiamen, China), according to the manufacturer's protocol. RT-PCR was performed with the Novel Coronavirus (2019-nCoV) Nucleic Acid Diagnostic Kit (PCR-Fluorescence Probing; Ref. No. S3102E; Sansure Biotech, Changsha, China). According to the manufacturer's protocol and the study of Xu *et al.*,<sup>13</sup> the typical S-shape amplification curve detected at the ROX [nucleocapsid protein (N) gene] channel with a Ct value of  $\leq 40$  was considered to indicate SARS-COV-2 positivity.

#### RNA *IN-SITU* HYBRIDISATION

SARS-CoV-2 RNA in paraffin-embedded lung tissue was detected by the use of RNAscope *in-situ* hybridisation technology, according to the manufacturer's protocol. The reagents used in this study included RNAscope 2.5 HD Reagent Kit-Brown (Cat. No. 322300) and the RNAscope probe (Cat. No. 848561, V-nCoV2019-S, targeting the 21 631–23 303 region of NC\_045512.2), which were purchased from Advanced Cell Diagnostics (a Bio-Techne brand, Newark, CA, USA). In brief, deparaffinised tissue sections were treated with RNAscope Hydrogen Peroxide solution and subjected to target retrieval with the RNAscope Target Retrieval reagent. Dried slides were then incubated with RNAscope Protease Plus at 40°C for 15 min, and hybridised with the RNAscope probe (V-nCoV2019-S) at 40°C for 2 h. Hybridise AMP 1–6 reagents were further used to amplify the probe signals. The positive signals were stained with 3,3'-diaminobenzidine (DAB) and slightly counterstained with haematoxylin.

#### IMMUNOHISTOCHEMISTRY

Formalin-fixed paraffin-embedded tissue sections (4  $\mu$ m) were obtained for immunohistochemical

staining according to the standard protocol. Briefly, deparaffinised and rehydrated sections were treated with 3% hydrogen peroxide and subjected to antigen retrieval with citrate buffer (pH 6.0). Sections were blocked with 5% bovine serum albumin for 20 min, and incubated overnight with primary antibody at 4°C. Primary antibodies against cell markers used in this study included anti-CD3, anti-CD4, anti-CD8, anti-CD19, anti-CD20, anti-CD56, anti-CD68, anti-CD163, anti-multiple myeloma oncogene-1 (MUM1, also called IRF4), anti-paired box gene 5 (PAX5), anti-pan-cytokeratin (PCK), and anti-thyroid transcription factor 1 (TTF1), which were purchased from Dako (Carpinteria, CA, USA). Antibody binding to the cells in sections was detected with horseradish peroxidase reaction kits (Dako) according to the manufacturer's instructions. The reaction products were stained with DAB and slightly counterstained with haematoxylin.

## Results

### LABORATORY FINDINGS

Baseline complete blood counts, biochemistry, coagulation studies and immune cell analysis are shown in Tables S1 and S2.

### GROSS PATHOLOGY

Two fragments of lung tissue were obtained from the right lower lobectomy, measuring 125 × 57 × 30 mm and 119 × 90 × 35 mm. No areas of consolidation or nodular lesions could be found on gross examination.

### DETECTION OF SARS-COV-2 IN LUNG TISSUE

Real-time RT-PCR performed on the lung tissue showed a Ct value of 36.18 at the ROX (N gene) channel. RNA *in-situ* hybridisation performed on the lung tissue sections showed that the positive signals were brown in colour and located in the cytoplasm at the light-microscopic level (Figure 3A). In addition, at higher magnification of H&E staining, intracytoplasmic viral-like inclusions could be identified in a few type II pneumocyte-like cells (Figure 3B) or macrophage-like cells (Figure 3C). These viral-like inclusions were light red globules approximately half the size of an erythrocyte, and were surrounded by clear halos. These results demonstrated the presence of SARS-CoV-2 in the lung tissue, and thus confirmed that the patient was infected with SARS-CoV-2 preoperatively.

### HISTOPATHOLOGY

Near the visceral pleura, features of viral pneumonia were noted, mainly characterised by exudative inflammation. The closer to the visceral pleura, the more severe the exudation of monocytes and lymphocytes (Figure 4A). The inflammatory cells were centred on small blood vessels, and further infiltrated the surrounding alveolar septa and spaces (Figure 4B). The alveolar septa were widened, with obvious hyperaemia and dilation of capillaries. Interstitial fibrosis was rarely present. In the alveolar spaces, there were many monocytes, a few lymphocytes, and variable numbers of red blood cells forming clumps (Figure 4C). Multinucleated giant cells were also seen in a few alveolar spaces (Figure 4D). Neither fibrinous exudate nor hyaline membrane formation was

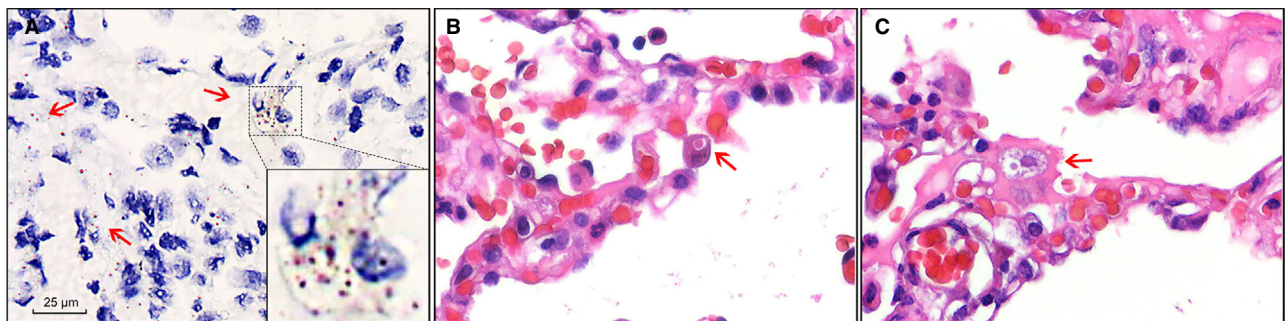


**Figure 3.** Detection of severe acute respiratory syndrome coronavirus 2 (SARS-CoV-2) in lung sections. A, SARS-CoV-2 RNA was detected with RNA *in-situ* hybridisation in lung sections. The positive signals (arrow) were brown in colour and were mainly located in the cytoplasm. Scale bar: 25 µm. Inset: higher magnification of the positive signals. B, An intracytoplasmic viral-like inclusion body seen in an enlarged epithelial cell (arrow) [haematoxylin and eosin (H&E)]. C, An intracytoplasmic viral-like inclusion body seen in a macrophage-like cell (arrow) (H&E).

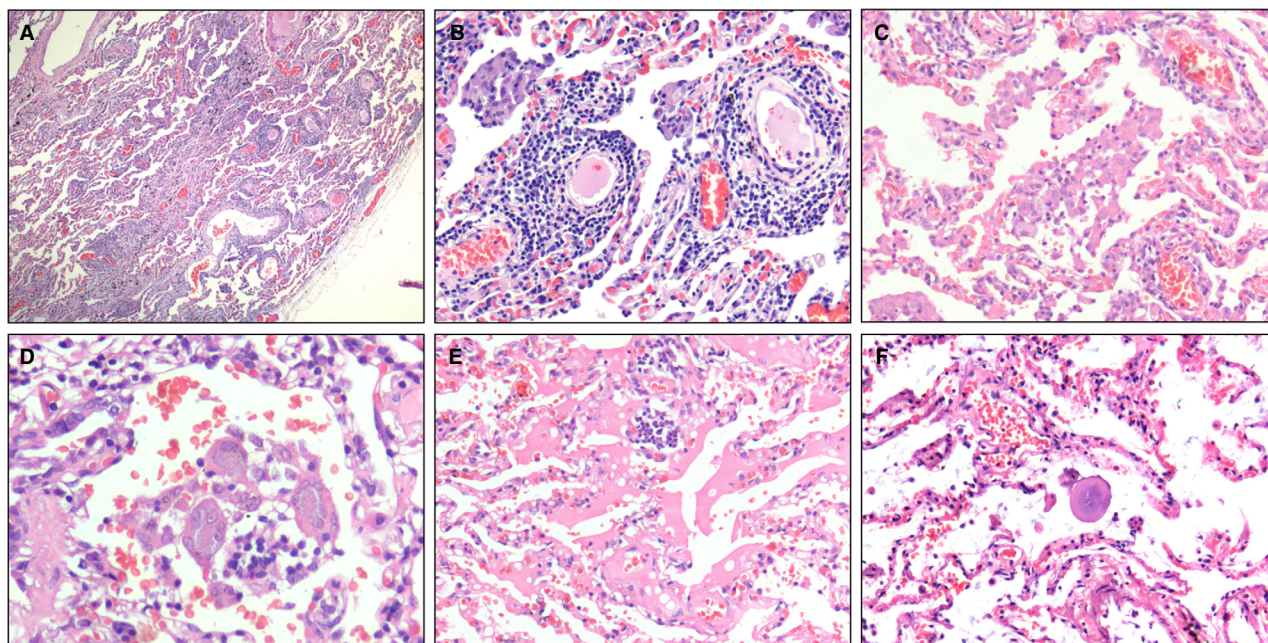


**Figure 4.** Pulmonary histomorphology. A, The closer to the visceral pleura, the more severe the exudation of inflammatory cells [haematoxylin and eosin (H&E)]. B, Perivascular inflammatory infiltration (H&E). C, A large number of monocytes, a few lymphocytes and variable numbers of red blood cells were present in the alveolar spaces (H&E). D, Intra-alveolar multinucleated giant cells (H&E). E, An area of serous exudation (H&E). F, An intra-alveolar large protein globule (H&E).

observed. Also, areas of serous exudation with pulmonary oedema were found. In these areas, some alveolar spaces were filled with a large amount of light red, homogeneous, proteinaceous fluid, admixed with variable numbers of red blood cells, lymphocytes, and monocytes (Figure 4E). In addition, scattered large protein globules in alveolar spaces were seen (Figure 4F). The bronchial structure remained intact. At higher magnification, there was focal hyperplasia of type II pneumocytes, some of which showed mild cytological atypia (Figure 5A). Some enlarged pneumocytes showed abundant cytoplasm with a ground-glass appearance, and prominent eosinophilic nucleoli (Figure 5B,C).

The pulmonary nodule near the hilum detected by the use of preoperative CT was demonstrated in the lobectomy specimen to be a meningothelial-like nodule with extensive thick-walled vessels. The COVID-19-related histopathological changes as described above were mild in this area. Only capillary dilation and congestion was seen around the nodule (Figure S1).

#### IMMUNOHISTOCHEMICAL FINDINGS

The inflammatory cells infiltrating the blood vessels and alveolar wall were mainly T lymphocytes (CD3+), with a few B lymphocytes (CD20+ and

PAX5+) and plasma cells (MUM1+) (Figure 6A–F). In order to further understand the role of T lymphocytes in this viral pneumonia, we used the surface markers of T lymphocytes to identify the subtypes. Immunohistochemistry confirmed that the predominant component was composed of CD4+ helper T lymphocytes, whereas CD8+ cytotoxic T lymphocytes and natural killer cells (CD56+) were scattered (Figure 6G–I).

Subsequently, we examined the expression of PCK and TTF1, which are markers of alveolar epithelial cells. Although the alveolar septa were infiltrated by lymphocytes, the alveolar structure was essentially intact, as highlighted by immunostaining (Figure 7A–C). The enlarged cells with amphophilic granular cytoplasm and prominent nucleoli lining the alveolar spaces recognised on H&E staining were PCK+ (Figure 5C), confirming the presence of abnormal hyperplasia of type II pneumocytes.

In addition to hyperplasia of type II pneumocytes, clusters of macrophage-like cells were found in the alveolar spaces (Figure 7A), which could be attributed to the desquamation of pneumocytes and recruitment of macrophages. Figure 7D shows that CD68+ macrophages were the main sources of cell clusters in the alveolar spaces. CD3+ T lymphocytes were also present (Figure 7E). In addition, immunostaining for CD163, a marker of M2 macrophages, showed strong

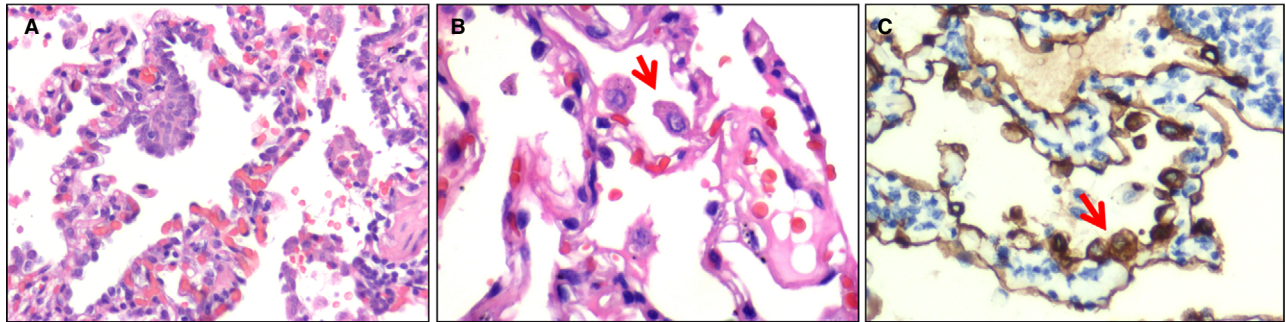


**Figure 5.** Atypical pneumocytes. A, High-power view of pneumocyte hyperplasia [haematoxylin and eosin (H&E)]. B, High-power view showing an enlarged pneumocyte (arrow) with amphophilic granular cytoplasm and a prominent eosinophilic nucleolus (H&E). C, Immunohistochemical staining showing atypical pneumocytes to be positive for pan-cytokeratin (arrow), confirming their epithelial origin (streptavidin peroxidase). [Colour figure can be viewed at [wileyonlinelibrary.com](http://wileyonlinelibrary.com)]

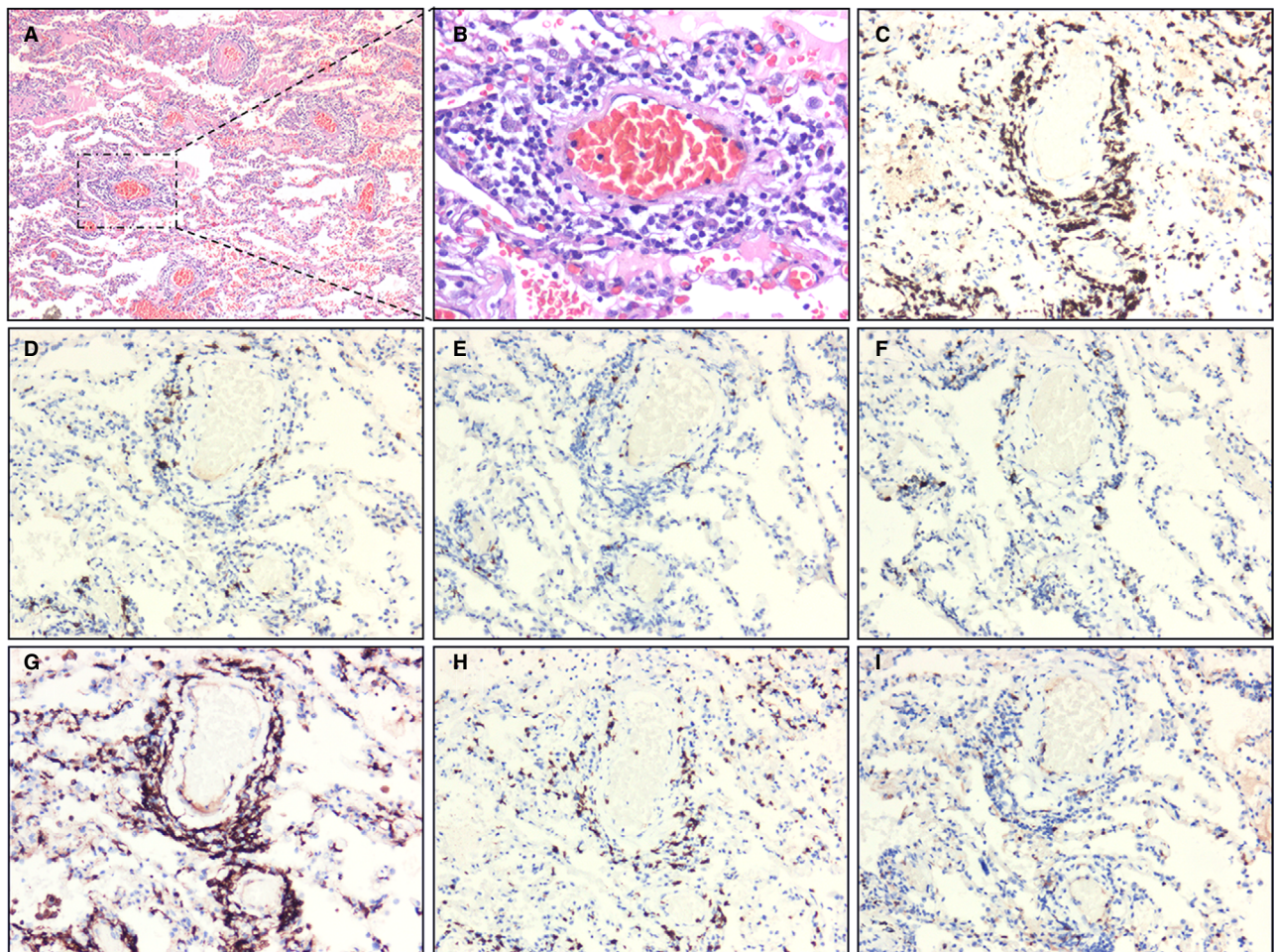


**Figure 6.** Immunohistochemical staining of lymphocytes. A, Extensive vasodilation and congestion in lung tissue. The interstitium was widened by oedema and inflammatory cell infiltrates. The alveoli were filled with serous fluid and red blood cells [haematoxylin and eosin (H&E)]. B, Monocytes and lymphocytes around blood vessels (H&E). C, CD3+ T lymphocytes (H&E) and CD20+ and paired box gene 5 (PAX5)+ B lymphocytes. F, Multiple myeloma oncogene-1 (MUM1)+ plasma cells. G, CD4+ helper T lymphocytes. H, CD8+ cytotoxic T lymphocytes. I, CD56+ natural killer cells (streptavidin peroxidase). [Colour figure can be viewed at [wileyonlinelibrary.com](http://wileyonlinelibrary.com)]

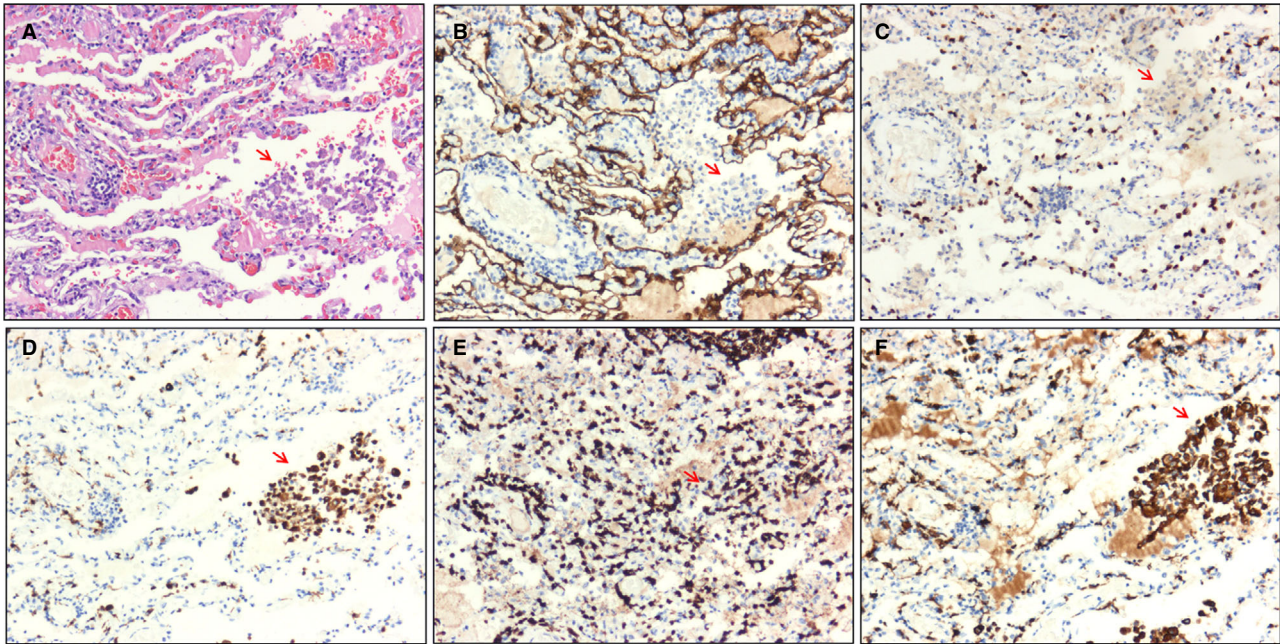


**Figure 7.** Immunohistochemical staining of intra-alveolar cells (arrow). A, Cell clusters consisting of macrophage-like cells seen in alveolar spaces [haematoxylin and eosin (H&E)]. B,C, Pan-cytokeratin (PCK)+ and thyroid transcription factor 1 (TTF1)+ alveolar epithelial cells were not detected in intra-alveolar cell clusters (streptavidin peroxidase). D, CD68+ macrophages were found in alveolar spaces (streptavidin peroxidase). E, CD3+ T lymphocytes were found in alveolar spaces (streptavidin peroxidase). F, Immunohistochemical staining of CD163 showed that most macrophages were of the M2 type (streptavidin peroxidase). [Colour figure can be viewed at [wileyonlinelibrary.com](http://wileyonlinelibrary.com)]

positivity and site-specific expression, suggesting that M2 macrophages may play a role in pathogenesis (Figure 7F).

## Discussion

The mean incubation period for SARS-CoV-2 infection is 5.2 days. In its early stage, the epidemic doubles every 7.4 days, with a mean serial interval of 7.5 days.<sup>14</sup> Our patient had no symptoms or other underlying diseases before lung surgery. She developed fever on postoperative day 2, and laboratory tests showed a decreased lymphocyte count and an increased WBC count in the peripheral blood, which could be easily confused with a stress response to surgery. However, her WBC and lymphocyte counts continued to decrease, and chest CT showed evidence of viral pneumonia. The diagnosis of preoperative COVID-19 was finally established by the use of real-time PCR and RNA *in-situ* hybridisation for the virus in the lung tissue. Given the combination of epidemiological characteristics, clinical presentation, nucleic acid testing, and intracytoplasmic viral-like inclusions, it is reasonable to speculate that this case represents an early stage of lung injury secondary to SARS-CoV-2 infection.

The main histological findings in the lung in this case included: (i) serous exudation; (ii) infiltration of lymphocytes around blood vessels and in the alveolar septa; (iii) aggregation of monocytes and multinucleated giant cells within alveolar spaces; (iv) hyperplasia of type II pneumocytes; and (v) intracytoplasmic viral-like inclusion bodies. In our opinion, the presence of intracytoplasmic viral-like inclusions may be one of the most useful features in the diagnosis of COVID-19 pneumonia. It correlates with electron-microscopic findings reported by Zhu *et al.*, that viral particles are present in membrane-bound vesicles in the cytoplasm.<sup>8</sup> Although they are approximately half the size of SARS viral inclusions, they are found in enlarged cells, similarly to SARS viral inclusions.<sup>15–18</sup> Further studies are needed to confirm this observation.

The primary pathology of both SARS and MERS in the lungs is diffuse alveolar damage (DAD).<sup>15</sup> Specifically, the SARS lungs show acute exudative DAD with extensive oedema and hyaline membrane formation in the early phase.<sup>16,17</sup> Subsequently, fibrous organisation follows, depending on the duration of SARS.<sup>16</sup> In our case of COVID-19, however, only serous exudate, rather than fibrinous exudate, was observed in the alveolar spaces. Hyaline membrane

formation was not observed, which is similar to the pulmonary pathology of early-phase COVID-19 pneumonia reported by Tian *et al.*<sup>11</sup> Interestingly, Xu *et al.* observed features of DAD with hyaline membrane formation in the late stage of COVID-19 pneumonia.<sup>12</sup> Therefore, we consider that hyaline membrane formation may be a time-dependent pathological process, and that the patient in our case might have been in the exudative phase of DAD, too early for obvious hyaline membrane formation. Moreover, considering that our case showed sharply decreased blood oxygen saturation and serious dyspnoea later, it is likely that she may have also progressed to full-blown DAD by the time of death. Unfortunately, we did not obtain permission for an autopsy to confirm this.

The pathophysiology of SARS is related to dysfunction of the immune system, including hyperinduction of chemokines and cytokines, an abnormal cellular immune response, and an insufficient interferon reaction.<sup>18–21</sup> Our studies provide evidence that a dysfunctional immune system may also be involved in the pathogenesis of COVID-19. Like SARS-CoV,<sup>20,22</sup> SARS-CoV-2 could directly attack epithelial cells, leading to hyperplasia of type II pneumocytes. The inflammatory cells (mainly CD4+ T lymphocytes) that infiltrate the blood vessels and alveolar wall in the lungs could cause abnormal release of cytokines (cytokine storm).<sup>18–21</sup> In addition, the decrease in the number of CD4+ T lymphocytes in the peripheral blood of this case suggests an abnormal redistribution between peripheral blood and lung tissue. SARS-CoV-2 may also trigger chemotactic movement of macrophages, as indicated by macrophage aggregates within alveolar spaces.

In summary, we report the histopathological findings in lung tissue from a patient with an established diagnosis of COVID-19. We believe that the findings represent changes seen in the early stage of the disease, in contrast to those observed at autopsy. Our data also suggest that immune dysfunction is implicated in the pathogenesis of SARS-CoV-2 infection.

### Conflicts of interest

The authors declare that they have no conflicts of interest.

### Funding

This work was supported by a grant from the National Natural Science Foundation of China (Grant No. 81602535).

### Compliance of ethical standards

The study (WDRY2020-K005) was approved by the Ethics Committee of Renmin Hospital of the Wuhan University, and was performed in accordance with the ethical standards laid down in the 1964 Declaration of Helsinki and its later amendments. Written informed consent was waived by the same committee.

### Author contributions

Jing-ping Yuan and Wan-li Jiang conceived and designed the study. Zhi Zeng and Xiao-yu Xie wrote the paper. Zhi Zeng and Jing-ping Yuan evaluated the immunohistochemical staining results. Hong-lin Yan and Xin-an Liu performed real-time RT-PCR. Li Xu performed RNA *in-situ* hybridisation. Bao-jun Xie, Wan-zhou Xu and Ganjun Kang reviewed and collected electronic medical records, pathological sections, laboratory findings, and chest CT findings. All authors contributed to manuscript revision, and read and approved the submitted version.

### Acknowledgements

We thank Professor Hanlin Wang (Department of Pathology, David Geffen School of Medicine, University of California, Los Angeles, CA, USA) for reviewing the manuscript and figures. We also thank Professor Changxin Jiang (Department of Pathology, Tianjin Medical University) and Professor Shanyou Peng (Department of Pathology, Renmin Hospital of Wuhan University) for reviewing the tissue sections.

### References

1. Chan JF, To KK, Tse H, Jin DY, Yuen KY. Interspecies transmission and emergence of novel viruses: lessons from bats and birds. *Trends Microbiol.* 2013; 21: 544–555.
2. *Summary of probable SARS cases with onset of illness from 1 November 2002 to 31 July 2003.* World Health Organization. Available at: [https://www.who.int/csr/sars/country/table\\_2004\\_04\\_21/en/](https://www.who.int/csr/sars/country/table_2004_04_21/en/) (accessed 8 March 2020).
3. *Middle East respiratory syndrome coronavirus (MERS-CoV).* World Health Organization. Available at: <http://www.who.int/emergencies/mers-cov/en/> (accessed 8 March 2020).
4. *Update on the novel coronavirus pneumonia outbreak.* China National Health Commission. Available at: <http://www.nhc.gov.cn/xcs/yqtb/202004/c5c446c763184509ad8baae9f748ab74.shtml> (accessed 24 April 2020).
5. Holshue ML, DeBolt C, Lindquist S *et al.* First case of 2019 novel coronavirus in the United States. *N. Engl. J. Med.* 2020; 382: 929–936.
6. Park WB, Kwon NJ, Choi SJ *et al.* Virus isolation from the first patient with SARS-CoV-2 in Korea. *J. Korean Med. Sci.* 2020; 35: e84.

7. COVID-19 coronavirus outbreak. Worldometer. Available at: <https://www.worldometers.info/coronavirus/> (accessed 11 March 2020).
8. Zhu N, Zhang D, Wang W *et al*. A novel coronavirus from patients with pneumonia in China, 2019. *N. Engl. J. Med.* 2020; **382**: 727–733.
9. Zhou P, Yang XL, Wang XG *et al*. A pneumonia outbreak associated with a new coronavirus of probable bat origin. *Nature* 2020; **579**: 270–273.
10. Huang C, Wang Y, Li X *et al*. Clinical features of patients infected with 2019 novel coronavirus in Wuhan. *China. Lancet* 2020; **395**: 497–506.
11. Tian S, Hu W, Niu L, Liu H, Xu H, Xiao SY. Pulmonary pathology of early-phase 2019 novel coronavirus (COVID-19) pneumonia in two patients with lung cancer. *J. Thorac. Oncol.* 2020; **15**: 700–704.
12. Xu Z, Shi L, Wang Y *et al*. Pathological findings of COVID-19 associated with acute respiratory distress syndrome. *Lancet Respir. Med.* 2020; **8**: 420–422.
13. Xu SP, Kuang D, Hu Y, Liu C, Duan YQ, Wang GP. Detection of 2019-nCoV in the pathological paraffin embedded tissue. *Zhonghua Bing Li Xue Za Zhi* 2020; **49**: E004.
14. Li Q, Guan X, Wu P *et al*. Early transmission dynamics in Wuhan, China, of novel coronavirus-infected pneumonia. *N. Engl. J. Med.* 2020; **382**: 1199–1207.
15. Tse GM, To KF, Chan PK *et al*. Pulmonary pathological features in coronavirus associated severe acute respiratory syndrome (SARS). *J. Clin. Pathol.* 2004; **57**: 260–265.
16. Cheung OY, Chan JW, Ng CK, Koo CK. The spectrum of pathological changes in severe acute respiratory syndrome (SARS). *Histopathology* 2004; **45**: 119–124.
17. Lang ZW, Zhang LJ, Zhang SJ *et al*. A clinicopathological study of three cases of severe acute respiratory syndrome (SARS). *Pathology* 2003; **35**: 526–531.
18. Regla-Nava JA, Jimenez-Guardeno JM, Nieto-Torres JL, Gallagher TM, Enjuanes L, DeDiego ML. The replication of a mouse adapted SARS-CoV in a mouse cell line stably expressing the murine SARS-CoV receptor mACE2 efficiently induces the expression of proinflammatory cytokines. *J. Virol. Methods* 2013; **193**: 639–646.
19. He L, Ding Y, Zhang Q *et al*. Expression of elevated levels of pro-inflammatory cytokines in SARS-CoV-infected ACE2+ cells in SARS patients: relation to the acute lung injury and pathogenesis of SARS. *J. Pathol.* 2006; **210**: 288–297.
20. Shi CS, Qi HY, Boullaran C *et al*. SARS-coronavirus open reading frame-9b suppresses innate immunity by targeting mitochondria and the MAVS/TRAF3/TRAF6 signalosome. *J. Immunol.* 2014; **193**: 3080–3089.
21. Liu WJ, Zhao M, Liu K *et al*. T-cell immunity of SARS-CoV: implications for vaccine development against MERS-CoV. *Antiviral Res.* 2017; **137**: 82–92.
22. Ding Y, Wang H, Shen H *et al*. The clinical pathology of severe acute respiratory syndrome (SARS): a report from China. *J. Pathol.* 2003; **200**: 282–289.

## Supporting Information

Additional Supporting Information may be found in the online version of this article:

**Figure S1.** Histomorphology of the pulmonary nodule near the hilum detected with preoperative CT.

**Table S1.** Baseline full blood count results.

**Table S2.** Biochemistry, coagulation study and immune cell analysis results.